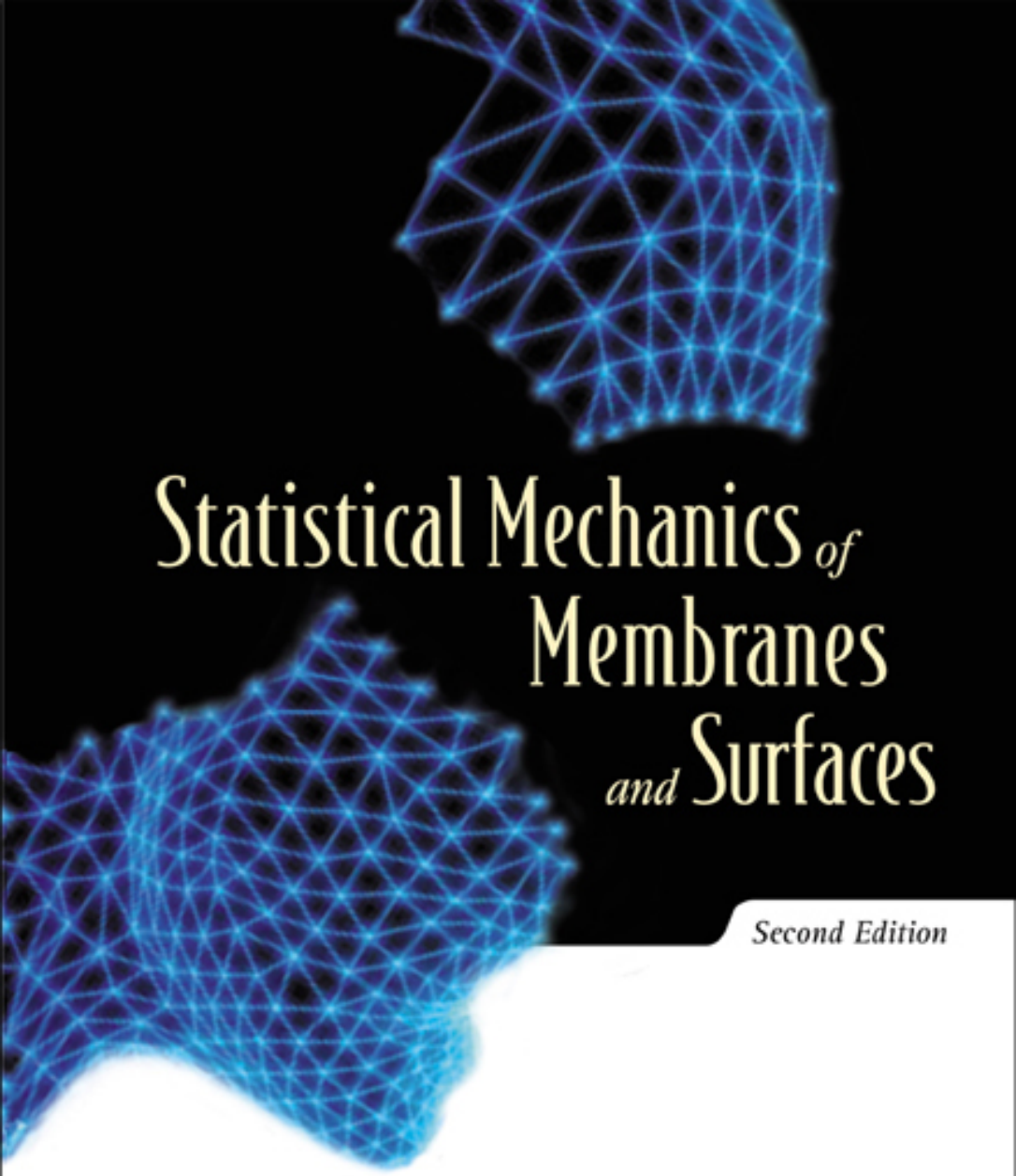

Statistical Mechanics of Membranes and Surfaces

Second Edition

Edited by

D. Nelson · T. Piran · S. Weinberg

CHAPTER 5

PROPERTIES OF TETHERED SURFACES

Yacov Kantor

School of Physics and Astronomy,
Tel Aviv University, Tel Aviv, Israel

The statistical mechanics of polymerized surfaces is discussed. The radius of gyration, R_g, of a model system, representing a flexible surface without excluded volume interactions, increases as $\sqrt{\ln L}$, where L is the linear size of uncrumpled surface, i.e., the surface overfills the embedding space. With excluded volume interactions the surface expands but remains very crumpled and its R_g increases as L^ν, with $\nu \approx 0.8$, in a three-dimensional space. Very rigid surfaces are asymptotically flat. As the rigidity of the surface varies, it undergoes a second order phase transition with diverging specific heat from a crumpled to a flat state. These lecture notes stress the analogies and relations between the surfaces and D-dimensional manifolds and branched polymers.

1. Introduction

1.1. *What is a "Tethered Surface"?*

Recently there have been many studies of random two-dimensional surfaces. (For a review, see Frölich (1985).) Some studies focused on random surfaces related to high-temperature plaquette expansions of lattice gauge theories (see, e.g., Parisi (1979), Drouffe *et al.* (1979)), while others stressed the properties related to condensed matter physics, such as the behavior of membranes (see, e.g., Helfrich (1987), and references therein). However, there is no single universality class encompassing all surfaces (Cates, 1985a). It is, therefore, important to clearly define the type of surface one is considering.

In these lecture notes, I consider a system of particles (atoms or monomers) that are connected to form a regular two-dimensional array embedded in d-dimensional space. The precise type of the two-dimensional lattice is not important. Figure 1 depicts a triangular network of particles in a three-dimensional space. The precise form of the "bonding potential" between the neighboring particles of the network is also unimportant. However, it is essential that the bonds between the adjacent atoms or monomers of the array cannot be broken. This feature is typical for many polymeric structures, where at the experimentally relevant temperatures the

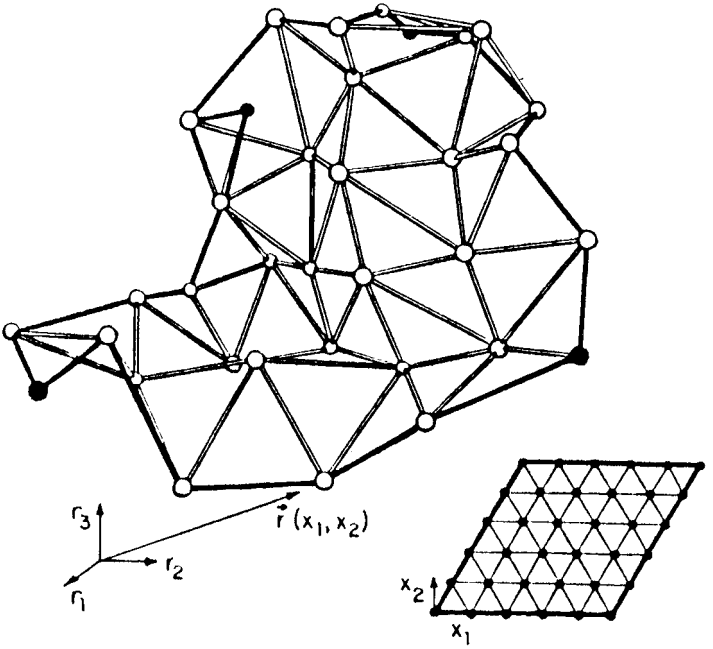

Fig. 1. Triangular tethered surface embedded in a three-dimensional space. The picture in the lower right corner depicts the topology (connectivity) of the surface. Positions of the particles in the internal (two-dimensional) coordinate space are determined by vector $\mathbf{x}$. The actual positions of the particles as shown in the main figure are the three-dimensional external coordinates $\mathbf{r}(\mathbf{x})$. Boundary bonds and corner particles are shown in black.

bonds are practically unbreakable. Thus, the surfaces preserve their *connectivity* and will be denoted "tethered (or polymeric) surfaces" (Kantor *et al.*, 1986). Such objects can be created by cross-linking of monomers on liquid-liquid, or liquid-gas, or solid-gas interfaces. A typical example of such a structure is cross-linked poly(methyl methacrylate) extracted from the surface of sodium montmorillonite clays (Blumstein *et al.*, 1969). Alternatively, polymeric surfaces can be obtained by cross-polymerization of lipid bilayers (see, e.g., Fendler and Tundo (1984)).

The physical properties of tethered surfaces differ significantly from the properties of *liquid* surfaces. In particular we shall see that the tethered surfaces may be in both crumpled and flat states, while the liquid surfaces are always crumpled beyond a certain persistence length. One can understand the origin of the differences by considering a simple example: Suppose we are trying to "fold" a flat surface of size $L \times L$ into a spherical shell of the same area. Clearly, one cannot perform such folding with a piece of paper (without cutting it) since it requires stretching and compression of various areas of the sheet. On the other hand, if we allow a free motion of the molecules along the surface (i.e., remove the fixed connectivity constraint), such "folding" will become possible. Thus, the fixed connectivity is an essential part of the model described in these lecture notes.

1.2. *The Tethered Surface as a Polymer*

Fixed connectivity of tethered surfaces provides some conceptual and technical advantages:

(a) The infinite strength of the bonds within the surface ensures the integrity of that object. One can, at least in principle, consider a *single* surface with definite microscopic interactions, and deduce the long wavelength behavior of the surface. Unlike its liquid counterparts, a single polymeric surface cannot evaporate even in the absence of external pressure or external reservoir of monomers, i.e. a "freely suspended" tethered surface is in a true thermodynamic equilibrium.

(b) Fixed connectivity provides a convenient and natural way to describe the surface. In this sense, the tethered surface closely resembles a linear polymer. The spatial conformation of a linear polymer can be described by a set of position vectors $\mathbf{r}(x)$, where x is the internal index (number of a monomer along the chain), while $\mathbf{r}$ is the position of that monomer. A natural generalization for a two-dimensional surface, is made by using a *two-dimensional* vector $\mathbf{x}$ which denotes the *internal* position of the atom (i.e., its location within the array), as depicted in Fig. 1. Such use of a fixed (flat) internal space, and its clear separation from the external variable $\mathbf{r}$, on which the Hamiltonian of the system depends, enables an unambiguous definition of the statistical measure, thus avoiding some problems regarding a proper measure, which may occur in, say, liquid surfaces.

One should view a tethered surface not only as a member in the large family of two-dimensional objects, but also, as a particular case of a polymeric structure. It is very useful to consider the two-dimensional polymeric surface as a particular case of D-dimensional polymeric manifolds, or as a case of a branched polymer. Throughout these lecture notes, I will stress the analogies between these surfaces and other polymeric structures.

These notes are based on work which was done in collaboration with M. Kardar and D. R. Nelson. I have attempted to provide a self-contained description of the main features of these surfaces, and have stressed the main problems which have yet to be resolved. Since the subject is undergoing rapid development, I did not attempt to make its review exhaustive, but rather tried to supply the reader with the main references, where he can find a more detailed description.

The following section describes the behavior of oversimplified models for polymeric structures, which are both flexible and have no excluded volume interactions. Section 3 analyzes the effects of the excluded volume. Finally, bending rigidity is added to surfaces in Sec. 4, bringing the model close to realistic structures. In Sec. 5, I summarize the properties of the tethered surfaces and discuss the possible extensions and further directions in the development of this subject.

2. Phantom Chains and Networks

2.1. *Linear Polymers*

Linear polymers are formed by interconnection of a large amount of chemical (monomeric) units into a (topologically) linear structure, where each monomer is connected only to two other monomers. Despite the complexity of macromolecular structures, some of their properties are remarkably simple, and independent of their detailed chemical composition. (For a review, see, Flory (1979), de Gennes (1979).) The origin of such "universality" can be understood from the following idealized model: Consider a linear chain consisting of L freely-jointed rods, embedded in d dimensions. The length of each rod a is fixed, while the angle between the neighboring rods is not restricted (see, e.g., Weiner (1983)). Each spatial conformation of such a chain is a particular example of an L-step random walk. Since the vector connecting the end-points of the chain $\mathbf{r}$ is a sum of L independent individual step vectors, its probability distribution $p(\mathbf{r})$ approaches a Gaussian form

$$p(\mathbf{r}) \sim \mathrm{e}^{(-d/2La^2)r^2}, \tag{2.1}$$

as $L \to \infty$. Actually the probability distribution approaches its limiting form very fast, and for $L \sim 10$, it is already barely distinguishable from the Gaussian. This limiting behavior is a direct consequence of the central limit theorem, and does not depend on the binding potential between the neighboring monomers of the chain. For an arbitrary binding (central force) potential, (2.1) is the ultimate ($L \to \infty$) result, provided that a^2 in that expression is replaced by the mean-squared distance between a pair of neighboring monomers. Introduction of bending forces or restriction of the angles between the successive bonds of the chain complicates the treatment (see, e.g., Weiner (1983)), but results only in the replacement of a in (2.1) by an effective length ("Kuhn statistical segment"), and replacement of the actual number of monomers L by the number of Kuhn segments.

One may think of (2.1) as a statistical weight generated by a Hamiltonian

$$H = \frac{1}{2} k_B T \frac{d}{La^2} r^2 \tag{2.2}$$

of a "Gaussian spring", with a temperature dependent force constant. Notice, that it differs from a regular "Hookean spring", by the fact that it has a vanishing equilibrium length. It is important to realize the entropic origin of the behavior described by (2.2): The "spring-like" Hamiltonian (2.2) simply indicates, that when two ends of the molecule are brought closely together, the phase space available for the intermediate points of the chain is larger. This H essentially represents the $-TS$ term in the expression for the free energy $F = U - TS$, where U is the energy and S is the entropy.

It is convenient to subdivide a very long molecule into submolecules, each of which is large enough to be described by (2.2). The "energy" of the entire molecule

will now become a sum of the contributions of several Gaussian springs:

$$\frac{H}{k_BT} = \frac{1}{2}K_0 \sum_x [\mathbf{r}(x+a) - \mathbf{r}(x)]^2, \tag{2.3}$$

where x is the *internal* coordinate of a unit (monomer or submolecule), measuring its position along the chain, and a is the distance between the successive units. In the continuum limit (2.3) is replaced by

$$\frac{H}{k_BT} = \frac{1}{2}K \int \left(\frac{d\mathbf{r}}{dx}\right)^2 dx. \tag{2.4}$$

One should keep in mind, that here, and through the entire Sec. 2, we limit the interaction of a monomer to few neighboring monomers along the chain and completely disregard the interactions between the monomers located at the remote parts of the chain. An important omission of the model is the absence of the steric (or excluded volume, or self-avoiding) effect: In reality two monomers cannot occupy the same position in space, and must repel each other, when they come close together. (Of course, the details of the interaction also depend on the solvent in which the polymer is placed.)

2.2. *Gaussian Networks and Surfaces*

A natural generalization of a linear polymer is a network of Gaussian chains, such as depicted in Fig. 2. It is defined by a set of nodes $\{i\}$ connected by Gaussian springs with force constants K_{ij}, i.e., the Hamiltonian of the network is

$$\frac{H}{k_BT} = \frac{1}{2}\sum_{i,j} K_{ij}(\mathbf{r}_i - \mathbf{r}_j)^2. \tag{2.5}$$

Notice that (2.5) already *assumes* that the nodes are interconnected via *long* chains, described by "energies" proportional to the squared end-to-end distance. In general, we *cannot* prove, that a network of monomers with more realistic microscopic potential indeed approaches the form (2.5) on, say, sufficiently long length-scales.

The geometrical properties of Gaussian networks are extremely simple. Usually, one can calculate the mean-squared distance between two nodes, say l and m,

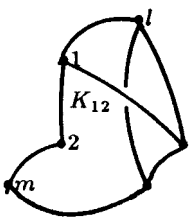

Fig. 2. Example of a network. Full circles (•) denote the nodes. For a Gaussian network, the lines depict the connecting springs. For a resistor network, the lines represent conductances K_{ij}.

since the thermal averaging of $(\mathbf{r}_l - \mathbf{r}_m)^2$ for the Hamiltonian (2.5) only requires calculation of the Gaussian averages:

$$\langle(\mathbf{r}_l - \mathbf{r}_m)^2\rangle = \frac{\int(\mathbf{r}_l - \mathbf{r}_m)^2 \mathrm{e}^{-H/k_BT} \prod_i d\mathbf{r}_i}{\int \mathrm{e}^{-H/k_BT} \prod_i d\mathbf{r}_i}. \tag{2.6}$$

This type of average can be easily performed for simple networks (see, e.g., Kardar and Nelson, 1988), such as periodic arrays of monomers. However, for more complicated networks, it is useful to notice a simple relation between this statistical-mechanical problem, and the conductivity problem in a resistor network. Such a relation has been known (in various forms) in polymer physics for quite some time, and has been used, in conjunction with various *approximations* to discuss entropic elasticity (see, e.g., Stauffer *et al.* (1982)). However, only recently it has been used (Cates, 1984, 1985b) to apply our understanding of the resistor networks to the field of polymer physics. In the absence of a convenient reference, I present a somewhat detailed proof of the *exact* relation.

Consider a resistor network with a connectivity defined in Fig. 2, where K_{ij} is the conductance of an elementary resistor connecting the nodes i and j. The two-point resistance $\mathcal{R}_{lm}$ between the nodes l and m equals the potential difference $\phi_l - \phi_m$ between the nodes divided by the current I which is injected in l and extracted at m. The potential difference can be found from the solution of Kirchhoff's circuit rules, which is equivalent to minimization of heat dissipation. Thus, the conductance problem is reduced to the minimization of S defined by

$$S \equiv S_0 - I(\phi_l - \phi_m), \tag{2.7a}$$

$$S_0 \equiv \frac{1}{2}\sum_{i,j} K_{i,j}(\phi_i - \phi_j)^2, \tag{2.7b}$$

where the second term on the r.h.s. of (2.7a) accounts for the fact that the minimization is performed under the restriction, that the current I is injected and extracted at l and m respectively, by an external current source. One can further replace the minimization of the quadratic form S by averaging with the Gaussian weight e^{-S} to obtain

$$\begin{aligned}\mathcal{R}_{lm} &= \left[\frac{\phi_l - \phi_m}{I}\right]_{\min\{S\}} = \frac{\int\left[\frac{\phi_l-\phi_m}{I}\right]\mathrm{e}^{-S}\prod_i d\phi_i}{\int \mathrm{e}^{-S}\prod_i d\phi_i} \\ &= \frac{\int(\phi_l - \phi_m)^2 \mathrm{e}^{-S_0}\prod_i d\phi_i}{\int \mathrm{e}^{-S_0}\prod_i d\phi_i}\end{aligned} \tag{2.8}$$

(cf., Stephen, 1978). We now notice that (2.6) and (2.8) almost coincide. Although (2.6) involves integrals over d-dimensional *vectors* $\mathbf{r}_i$, each component of the vectors can be integrated separately, and we essentially have d identical *scalar* integrals.

Thus we obtain a simple relation between the mean-squared distance in the statistical mechanics and the resistance:

$$\langle(\mathbf{r}_l - \mathbf{r}_m)^2\rangle = d\mathcal{R}_{lm}. \tag{2.9}$$

In polymer physics, one usually characterizes the spatial extent of a network by its squared radius of gyration

$$R_g^2 \equiv \frac{1}{2N^2}\sum_{i,j}\langle(\mathbf{r}_i - \mathbf{r}_j)^2\rangle. \tag{2.10}$$

In the case of a Gaussian network one may use (2.9) to relate this radius to the resistance of an analogous resistor network

$$R_{go}^2 = d\mathcal{R}. \tag{2.11}$$

Here, $\mathcal{R}$ is the two-point resistance averaged over all possible pairs of the nodes of the network. It is important to notice, that R_{go} strongly depends on the connectivity (topology) of the network, and, except for a trivial multiplicative factor, is independent of the dimension d of the embedding space.

The simplest generalization of a *linear* polymer is a D-dimensional manifold. $D = 1$ corresponds to a linear polymer, while $D = 2$ is a "regular" surface. We consider a manifold of internal dimensions $L \times L \times \cdots \times L$ (D times). It is convenient to index the monomers of the manifold in the internal coordinate space by a D-dimensional vector $\mathbf{x}$ (see Fig. 1). The general expression (2.5) now simplifies, since the summation now is performed only over the pairs of neighboring monomers of the manifold. In the continuum limit, a simple generalization of (2.4) is

$$\frac{H}{k_B T} = \frac{1}{2}K\int(\nabla\mathbf{r})^2 d^D\mathbf{x} \tag{2.12a}$$

$$(\nabla\mathbf{r})^2 \equiv \sum_{i=1}^{D}\left(\frac{\partial\mathbf{r}}{\partial x_i}\right)^2. \tag{2.12b}$$

The extent to which a manifold is crumpled in the embedding space can be characterized by the critical exponent ν, which relates the spatial extent of the manifold to its internal size L

$$R_g \sim L^{\nu}. \tag{2.13}$$

Alternatively, one can use the fractal dimension d_f (Mandelbrot, 1977, 1982) to relate the mass (number of monomers) of the manifold N to its size in the embedding space

$$N \sim R_g^{d_f}. \tag{2.14}$$

Since for a D-dimensional manifold $N = L^D$, these two indices are related by

$$\nu = D/d_f. \tag{2.15}$$

One can find the critical exponents for Gaussian manifolds either by a direct calculation of (2.6) with the Hamiltonian (2.12) (Kardar and Nelson, 1988) or by

a simple recollection of the distance (L) dependence of the potential produced by a point charge in electrostatics (or produced by a current inserted at a point in conducting medium) in D-dimensional space, and taking advantage of the relation (2.11). Either way one finds, for $D \leq 2$:

$$\nu_o = \frac{2-D}{2}, \tag{2.16a}$$

$$d_{fo} = \frac{2D}{2-D}, \tag{2.16b}$$

where the additional subscript o indicates that the exponents are related to the *Gaussian* manifolds.

For a two-dimensional surface ($D = 2$), the exponent ν_o vanishes and the fractal dimension is infinite, since for such manifolds

$$R_{go}^2 = \frac{d}{\pi K} \ln L. \tag{2.17}$$

One can visualize a surface as, say, a triangular network of Gaussian springs embedded in d dimensions (Kantor *et al.*, 1986). [A somewhat related, but not equivalent, model has been considered by Billoire *et al.* (1984) and Gross (1984).]

Networks with irregular connectivity usually cannot be solved analytically. However, one may take advantage of the fact that the *conductivity* of the numerous types of fractal structures, such as lattice animals, percolation clusters or cluster aggregates, has been investigated numerically. Typically, numerical investigations of fractals on the lattices are concerned with the establishment of a relation between the mean resistance $\mathcal{R}$ of such a fractal and its linear size (on the lattice) L, i.e. calculation of the critical exponent $\tilde{\zeta}$ defined by

$$R \sim L^{\tilde{\zeta}}. \tag{2.18}$$

The fractal dimension d_{fl}, which relates the mass of the fractal N to its linear size L *on the lattice* is also measured. These two exponents combined with the relation (2.11) suffice for the calculation of the radius of gyration R_{go} of a Gaussian network, which has the same *connectivity* as the lattice fractal. Thus for fractals we find

$$\nu_o = \tilde{\zeta}/2, \tag{2.19a}$$

$$d_{fo} = 2d_{fl}/\tilde{\zeta}. \tag{2.19b}$$

The exponent ν_o is not a very useful quantity for fractal networks, since it relates R_{go} to the *linear size of lattice fractal*, which depends on the choice of embedding of the network on a lattice: E.g., the same linear polymer can be represented on a lattice as a straight line and as a random walk, thus leading to different values of the linear size of the fractal, and to different values of ν_o. On the other hand, d_{fo} relates R_{go} to a physically well-defined mass N of the fractal. Since d_{fo} may depend only on the connectivity of the structure, while both d_{fl} and $\tilde{\zeta}$ depend on the particular

embedding, it is not surprising that d_{fo} depends only on the ratio between the two. Actually, it can be reexpressed in terms of spectral (or fracton) dimension (Alexander and Orbach, 1982; Rammal and Toulouse, 1983) $\tilde{d} \equiv 2d_{fl}/(\tilde{\zeta} + d_{fl})$:

$$d_{fo} = \frac{2\tilde{d}}{2 - \tilde{d}}. \tag{2.20}$$

Notice the relation between (2.16b) and (2.20) — the spectral dimension plays the role of the dimension of the manifold in the case of fractals.

2.3. *Properties of Phantom Tethered Surfaces*

In the previous subsection, I did not address the question, whether a tethered (two-dimensional) surface with realistic interatomic interactions approaches the Gaussian form (2.12) in the long wavelength limit. As an example, let us consider a triangular array of monomers embedded in a d-dimensional space, such as depicted in Fig. 1. The Hamiltonian with pairwise nearest-neighbor interactions is

$$\frac{H}{k_B T} = \sum_{\langle \mathbf{x}, \mathbf{x}' \rangle} V[\mathbf{r}(\mathbf{x}) - \mathbf{r}(\mathbf{x}')], \tag{2.21}$$

where $\mathbf{x}$ and $\mathbf{x}'$ are the *internal* coordinates of a pair of neighboring monomers, while $\mathbf{r}$'s are their positions in the *external* (embedding) space. Since the self-avoiding interactions between the distant parts of the surface are ignored, i.e., the surface can freely cross itself, it will be denoted "*phantom* surface".

In the previous subsection, I have shown that the model is solvable for $V(\mathbf{r}) = \frac{1}{2}K_0 r^2$. In particular, the radius of gyration of a finite surface is given by (2.17). Unfortunately, such a potential prefers the neighboring monomers to be located at the same point, and poorly represents any realistic microscopic interaction. Since other choices of $V(\mathbf{r})$ produce analytically unsolvable problems, we must resort to more approximate techniques. One such method is to construct an approximate renormalization group via Migdal–Kadanoff bond-moving approximation for integrating out the intermediate particles (Kadanoff, 1976). Since the high connectivity of a two-dimensional array prevents an exact rescaling, the Migdal–Kadanoff procedure replaces the actual connectivity by its approximation, i.e., the interactions are moved as shown in Fig. 3 to produce an isolated one-dimensional set of degrees of freedom. This *approximate* step conserves the number of bonds in the original problem and is followed by an *exact* decimation of a subset of particles.

It can be verified analytically that any Gaussian spring potential is exactly invariant under such transformation. We confirmed numerically (Kantor *et al.*, 1987) that several simple potentials converge to a Gaussian spring potential under the repeated application of Migdal–Kadanoff approximation.

Going beyond the approximate rescaling of the potential, the asymptotic Gaussian behavior was confirmed numerically by a Monte Carlo (MC) simulation

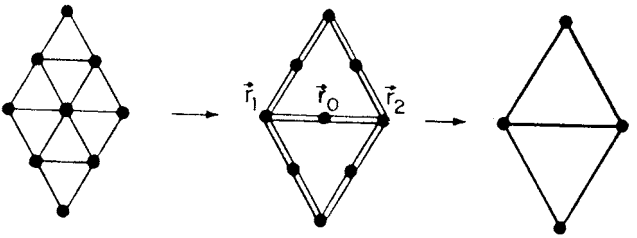

Fig. 3. Migdal–Kadanoff rescaling procedure for a triangular lattice: the first approximate step changes the connectivity of the lattice, and is followed by exact decimation.

(Kantor *et al.*, 1986, 1987). We considered a hard-sphere-and-string model with

$$V(\mathbf{r}) = \begin{cases} 0, & a < r < b \\ \infty, & \text{otherwise} \end{cases}. \tag{2.22}$$

Although the abrupt changes in the potential with increasing r are not realistic, it has, at least, the realistic feature of not allowing the neighboring monomers of the array to come too close together. Our model closely resembles models used to simulate linear polymers (see, e.g., Baumgärtner (1984)). Since our potentials do not introduce an energy scale into the problem, the results are independent of temperature and the free energy is due solely to entropic effects. We used the MC procedure to numerically equilibrate $L \times L$ parallelograms excised from a triangular lattice with free edges. The procedure was performed for L ranging from 2 to 16. The R_{go} has been measured as a function of L and has been found to approach a simple logarithmic behavior as L increased, i.e., the L-dependence coincided with the prediction (2.17) obtained for a Gaussian surface.

Although the numerical proof of the Gaussian behavior has been made for a particular type of potential $V(\mathbf{r})$ in $d = 3$, it is plausible to assume that it will be valid for any binding (central force) potential in an arbitrary d. Thus we shall use (2.12) as a starting point for the investigation of more realistic surfaces.

3. Excluded Volume Effects

3.1. *Bounds on the Exponent ν*

The next step towards a realistic description of surfaces is to consider the effects of self-avoiding interactions. One expects that introduction of such interactions will create larger (more open) structures. In particular, the exponent ν of such a structure should be larger than ν_o. Indeed, for linear polymers, $\nu \approx 0.59 > \nu_o = \frac{1}{2}$ in $d = 3$. The effect should be even more significant for two-dimensional surfaces, since in the absence of the excluded volume effects, their R_g barely depends on L (see Eq. (2.17)), and they overfill the embedding space ($d_{fo} = \infty$ for any d).

The physical limits on the values of ν are determined from a simple argument: Consider a two-dimensional surface of size $L \times L$ of finite thickness w in a

three-dimensional space. When the surface is stretched, its $R_g \sim L$. Since the volume of the surface is $L^2 w$, it can be "compactified" into an object of linear dimensions $\sim L^{2/3} w$. Thus, for such conformation, $R_g \sim L^{2/3}$. These two cases identify the physical bounds on the exponent ν: $\frac{2}{3} \leq \nu \leq 1$. Generally, for a D-dimensional surface in d-dimensional space:

$$\frac{D}{d} \leq \nu \leq 1, \tag{3.1a}$$

$$d \geq d_f \geq D. \tag{3.1b}$$

Are these, indeed, the best possible bounds, which can be obtained from simple geometric considerations? There are many ways to compactify a linear ($D = 1$) polymer in any d. However, the high connectivity of a two-dimensional surface restricts its possible spatial conformations, and it is not obvious that the compact conformation ($\nu = \frac{2}{3}$ in $d = 3$) can actually be attained. A "table-top experiment" (Kantor *et al.*, 1986, 1987; Gomes, 1987) in which sheets of foil have been "randomly" crumpled, showed that the diameter of the crumpled ball increased with the linear (uncrumpled) size of the sheet L as $L^{0.8}$, i.e., the resulting structure is *not* compact. Actually, it is quite difficult to find an "intelligent" (non-random) folding procedure, which will allow compactification of an arbitrarily large surface. (We assume, that the surface is elastic, and require that the elastic stretching energy required to compactify the surface increase slower than the surface area.) The reader is invited to try some simple folding procedures on a *very large* piece of paper, and to convince himself, that the task is not trivial. Nevertheless, at least one folding procedure (suggested by R. C. Ball), depicted in Fig. 4, succeeds in achieving that goal. Thus, the connectivity of the surface does not narrow down the bounds $\frac{2}{3} \leq \nu \leq 1$ for $D = 2$ and $d = 3$. We can only hope that similar foldings also exist for manifolds with $D > 2$ (for $d \geq D$), and, thus, (3.10) are the best possible bounds.

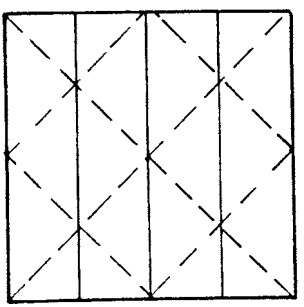

Fig. 4. Compactification of a two-dimensional sheet. The lines depict the creases created by the folds (of 180°) which can be seen if the sheet is unfolded back to a flat state. The solid and dashed lines indicate different directions of folding ("upwards" and "downwards"). Distances between the neighboring parallel creases are of order $L^{2/3} w^{1/3}$.

3.2. *Analytic Estimates of ν*

Excluded volume effects can be introduced into the continuum description of manifolds by generalizing Edwards' (1965) model for polymers (Kantor *et al.*, 1986). The full Hamiltonian now becomes

$$\frac{H}{k_BT} = \frac{1}{2}K\int(\nabla\mathbf{r})^2 d^Dx + \frac{1}{2}v\int\int\delta^d[\mathbf{r}(\mathbf{x})-\mathbf{r}(\mathbf{x}')]d^D\mathbf{x}d^D\mathbf{x}', \tag{3.2}$$

where the interaction ν measures the excluded volume effect. Dimensional analysis of (3.2) shows that for $D<2$ there exists an upper critical dimension

$$d_c(D) = \frac{4D}{2-D}, \tag{3.3}$$

such that for $d > d_c$ the excluded volume interactions are irrelevant, and ν and d_f are given by (2.16). For $D \geq 2$ self-avoidance is relevant in any d. The critical exponent at any point in the (D,d)-plane can (in principle) be evaluated by a systematic expansion from any point $(D^*, d_c(D^*))$ on the line of critical dimensions (3.3) (Kardar and Nelson, 1987, 1988; Aronovitz and Lubensky, 1987; Duplantier, 1987). To the lowest order in the "distance" from the line of critical dimensions, one finds

$$\nu(D,d) = \frac{2-D}{2} + \frac{2-D^*}{8[D^*+2C(D^*)]}\epsilon, \tag{3.4a}$$

$$\epsilon \equiv 4D-(2-D)d, \tag{3.4b}$$

$$C(D^*) \equiv \frac{\sqrt{\pi}\Gamma(2/(2-D^*))}{2^{2D^*/(2-D^*)}\Gamma((2+D^*)/2(2-D^*))}. \tag{3.4c}$$

Unfortunately, this expansion is too short to be useful for $D=2$ in $d=3$ since it predicts $\nu = 0.536$ (expansion around $d_c(D^*)=3$), which is certainly incorrect since it violates the bound (3.1). Thus, for the time being, we must rely on more approximate estimates.

The scaling behavior of self-avoiding polymers can be studied by Flory-type approximation (see, e.g., de Gennes (1979)). Consider a D-dimensional manifold of internal size L (and mass $N = L^D$), occupying a region of size R_g in the d-dimensional space. According to Flory, we may approximate the free energy F of the manifold by

$$\frac{F}{k_BT} = \frac{1}{2}\left(\frac{R_g}{R_{go}}\right)^2 + \frac{1}{2}v\left(\frac{N}{R_g^d}\right)^2 R_g^d. \tag{3.5}$$

The first term on the r.h.s. of (3.5) is the elastic (entropic) free energy of a *phantom* manifold (R_{go} is the radius of gyration of the manifold without self-avoidance). The second term is the mean-field estimate of the repulsive interaction energy (the squared density of the monomers $(N/R_g)^2$ is a mean-field-type estimate of the number of pair of monomers coming into close contact with each other in a unit

volume). By minimizing (3.5) and using (2.16) to relate R_{go} to L, we find $R_g \sim L^{\nu_F}$, with

$$\nu_F = \frac{D+2}{d+2}. \tag{3.6a}$$

Thus, the Flory estimate of the fractal dimension of the manifold is

$$d_{fF} = \frac{d+2}{D+2} D. \tag{3.6b}$$

In particular, for $D = 2$ and $d = 3$, we have $\nu_F = 4/5$ and $d_{fF} = 2.5$. Somewhat more formally, we can determine ν_F from (3.2) by requiring (Oono, 1981) that the rescaling factors of the internal coordinate $\mathbf{x}$ and the external coordinate $\mathbf{r}$ be related in such a way that the ratio between the two terms in (3.2) will remain unchanged under the rescaling.

For a more general case of a network with fractal connectivity (Cates 1984, 1985b), one can use (2.18) and (2.19), as well as the relation between N and L for a fractal, to obtain

$$d_{fF} = \frac{d+2}{\tilde{d}+2} \tilde{d}. \tag{3.7}$$

As in the then case of phantom networks, the expression (3.7) is obtained from (3.6b) by a substitution $D \to \tilde{d}$.

Despite its numerous deficiencies, the Flory-type theory produces remarkably good estimates of ν for linear polymers. Note that in the trivial cases of $d = D$ and $d = d_c(D)$, it produces exact answers. However, since it is an uncontrolled approximation, it is difficult *a priori* to assess its accuracy.

3.3. *Monte Carlo Investigation of Tethered Surfaces*

We performed a numerical (MC) equilibration of tethered surfaces with self-avoidance (Kantor *et al.*, 1986, 1987). As in the case of phantom surfaces, we equilibrated $L \times L$ parallelograms, with nearest neighbor interaction described by (2.22). However, now the repulsive (hard-core) interaction was "switched on" for any pair of monomers, i.e. no two monomers could come closer together than a distance a. The parameters in (2.22) were chosen to be $b/a = \sqrt{3}$, since such a choice ensures a complete impenetrability of the surface.

The size of equilibrated parallelograms L ranged from 2 to 11. Figure 5 depicts an equilibrium conformation of a self-avoiding surface. To study scaling properties of these surfaces, the R_g was calculated as a function of L. We found a nice power law dependence with $\nu \approx 0.83$.

The main source of possible errors in the simulation of such small surfaces are not the statistical errors, but rather "systematic errors" which appear since we are not in the asymptotic regime. Thus, it is useful to have two distinct ways to estimate ν, e.g. directly from the two-point (density-density) correlation function and from the "mass versus radius of gyration" curve. Differences in the exponents obtained by

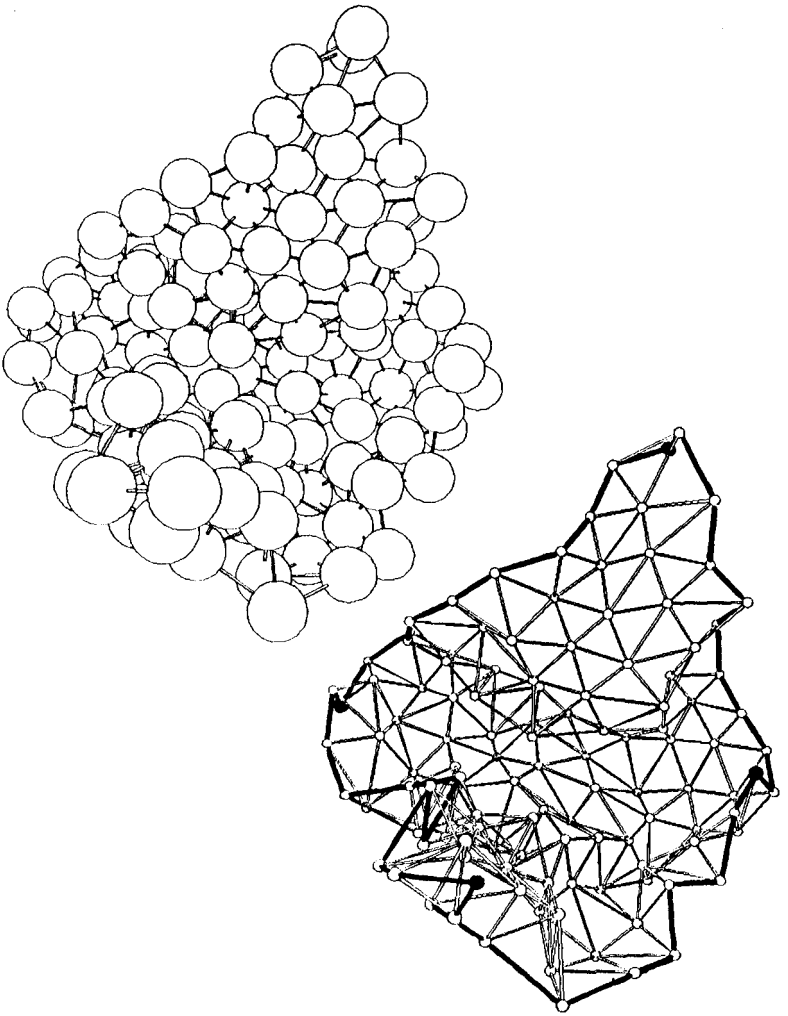

Fig. 5. Shape of the self-avoiding surface for $L = 11$ (top). Sphere sizes indicate the range of the repulsive potential. "Skeleton" of the same surface (bottom): For clarity, the sizes of the monomers (spheres) were taken to be $\frac{1}{5}$ of the actual range of the hard-core potential. Bonds indicate the nearest-neighbor atoms between which the "string" attractive potential acts. Boundary bonds and corner monomers are shown in black.

those methods provide an estimate of the "systematic error." We examined the Fourier transform of the two-point correlation function (or the structure factor)

$$S(\mathbf{k}, L) \equiv \frac{1}{L^4} \sum_{\mathbf{x},\mathbf{x}'} \langle \mathrm{e}^{i\mathbf{k}\cdot[\mathbf{r}(\mathbf{x})-\mathbf{r}(\mathbf{x}')]} \rangle. \tag{3.8}$$

In analogy with polymeric systems, we assume, that the structure factor satisfies the scaling form $S(\mathbf{k}, L) = S(kR_g) = S(kL^\nu)$. The lack of sphericity of the

self-avoiding surfaces is evident from Fig. 5, while our scaling relation for S assumed an isotropic **k**-dependence. The deviation from sphericity can be characterized by the ratio between the minimal and the maximal principal moments of inertia of the surface. This ratio was found to be ≈ 0.16, and *independent* (within the accuracy of the measurement) of L, thus justifying the use of spherically-symmetric scaling form. $S(0) \approx 1$ for $k < 1/R_g$, while for very large k ($k > 1$) we expect to have $S = 1/L^2$. To satisfy these conditions, as well as the scaling relation we must require $S \sim k^{-2/\nu}$ for $1 < k < 1/R_g$. From the k-dependence of S in this intermediate range of k's, we find $\nu \approx 0.77$. Thus, our overall estimate of ν is ~ 0.8. The corresponding fractal dimension is 2.5. This result is in good agreement with the Flory estimate $\nu_F = 4/5$, thus confirming the accuracy of the estimate and the physics embodied in (3.2).

4. Crumpling Transition in Tethered Surfaces

4.1. *Very Rigid and Very Flexible Surfaces*

What happens when we introduce bending rigidity into the tethered surfaces? In the previous sections, we ignored the rigidity and were led to the continuum descriptions (2.12) and (3.2) of the, respectively, phantom and self-avoiding surfaces. The $(\nabla r)^2$-term in those expressions does not represent the microscopic interactions, but results from a "coarse-graining" of the problem and is generated by the entropy in a crumpled surface. We might expect, that introduction of small rigidity will modify the persistence length, but will cause no change in the asymptotic behavior of the surfaces.

Investigations of the properties of very rigid surfaces usually take a point of view diametrically opposed to the crumpled surface ideas: One assumes that the surface is (at least locally) flat and describes its fluctuations using the Monge parametrization in terms of normal dispacement $f, \mathbf{r}(x_1, x_2) = (x_1, x_2, f)$. To the lowest order in f and its gradients, the surface energy may be written (Landau and Lifshitz, 1970)

$$F = \frac{1}{2}\tilde{\kappa} \int d^2x (\nabla^2 f)^2 + \frac{1}{2} \int d^2x (2\mu u_{ij}^2 + \lambda u_{kk}^2), \tag{3.9}$$

where the strain matrix u_{ij} is related to f and the in-plane displacements u_i by $u_{ij} = \frac{1}{2}(\partial_i u_j + \partial_j u_i + \partial_i f \partial_j f)$, $\tilde{\kappa}$ is the bending rigidity, and μ and λ are the in-plane Lamé constants. In *liquid* membranes the second term of (3.9) vanishes, and this leads to a crumpled surface, since the short wavelength transverse oscillations (undulations) reduce the effective rigidity of liquid surfaces on large length scales (Helfrich, 1985). However, it has been shown by an approximate (self-consistent) treatment of the vibrations, that in the presence of that term the transverse fluctuations are suppressed ($\langle f^2 \rangle$ increases slower than L^2), and the surface remains asymptotically flat (Nelson and Peliti, 1987).

Clearly, the results for very rigid and very flexible surfaces are not compatible, and one may expect a phase transition from a crumpled to a flat phase. We applied Monte Carlo methods to investigate the possibility of such a transition (Kantor and

Nelson, 1986, 1987). The model consisted of a hexagonal surface L monomers across, excised from a triangular lattice. The energy assigned to a particular conformation contained the nearest-neighbor interactions (2.22) and a bending energy term

$$\frac{H_b}{k_B T} = -\kappa \sum_{\langle \alpha,\beta \rangle} (\mathbf{n}_\alpha \cdot \mathbf{n}_\beta - 1), \tag{3.10}$$

where the sum is performed over pairs $\langle \alpha, \beta \rangle$ of adjacent unit normals $\{\mathbf{n}_\alpha\}$ erected perpendicular to each elementary triangle. Due to extremely long MC equilibration times, we did not attempt to include the excluded volume interactions into the model.

Figure 6 depicts the equilibrium conformations of the surface for several values of κ. We observe a dramatic change in the shape of the surface: For small values of κ, the surface overfills the space, as expected from flexible phantom surfaces. For large κ, the surface is quite "flat". We obtained quantitative evidence, supporting the claim that the observed effect is not a mere crossover. In particular, investigation of the L- and κ-dependence of R_g leads to the conclusion that for $L \to \infty$,

$$R_g(L) = \begin{cases} \xi\sqrt{\ln L} & \text{for } \kappa < \kappa_c \\ \zeta L & \text{for } \kappa > \kappa_c, \end{cases} \tag{3.11}$$

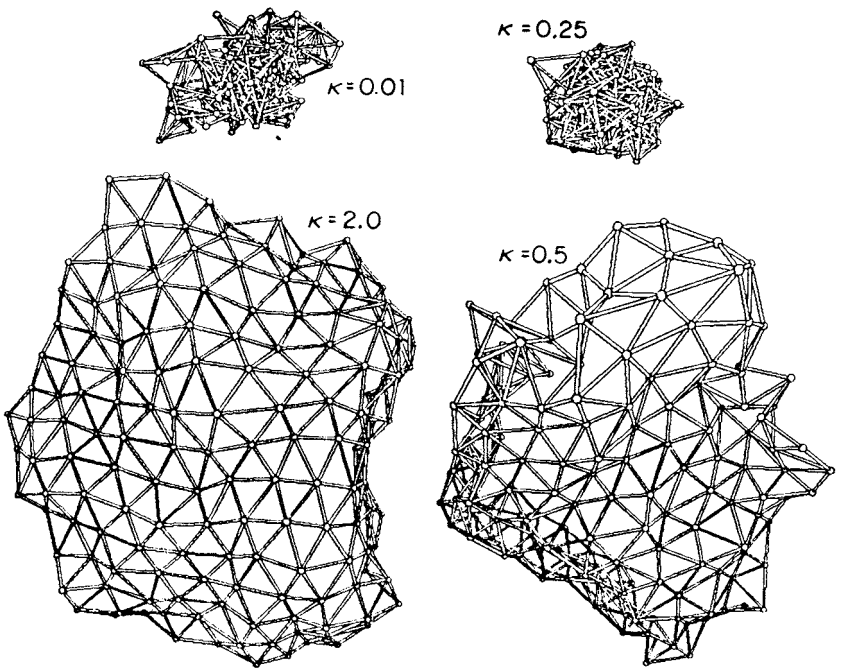

Fig. 6. Equilibrium conformations of hexagons $L = 15$ monomers across in the crumpled phase ($\kappa = 0.01$ and $\kappa = 0.25$), in flat phase ($\kappa = 2.0$), and close to the transition point ($\kappa = 0.5$).

where $\kappa_c \approx 0.33$. The values of ξ and ζ in (3.11) depend on κ: When κ approaches κ_c from below, the persistence length ξ increases and diverges at the transition point. The parameter ζ, which measures the possible shrinkage of the flat phase, decreases as κ approaches κ_c from above, and vanishes at the transition point. Precisely at the transition point κ_c (as well as away from κ_c, on length scales shorter than the correlation length), one may expect an intermediate "semicrumpled" regime, with $R_g \sim L^{\nu'}$. We indeed obtain such behavior with $\nu' \approx 0.8$.

However, the best evidence of the presence of the phase transition is provided by the specific heat measurements. Figure 7 depicts the κ-dependence of the specific heat per monomer C. For $\kappa = 0$ the fluctuations are purely entropic since the potential (2.22) allows only conformations with zero potential energy. Consequently, $C = 0$ at this point. (We suppress the trivial kinetic part $\frac{3}{2}k_B$ of the specific heat.) For sufficiently large κ, one can neglect the coupling between the transverse oscillations. [The two-dimensional (in-plane) degrees of freedom are entropic and do not contribute to the specific heat.] Therefore, for large κ we expect to obtain $C = \frac{1}{2}k_B$, in accordance with the Dulong–Petit law. Indeed all curves in Fig. 7 approach that limit for $\kappa \to \infty$. In the absence of a phase transition, one might expect a smooth interpolation of C as κ changes from 0 to ∞. On the other hand, we see a peak, which sharpens for large L. The position of the peak drifts towards small κ's as L increases and tends to a constant (positive) value κ_c.

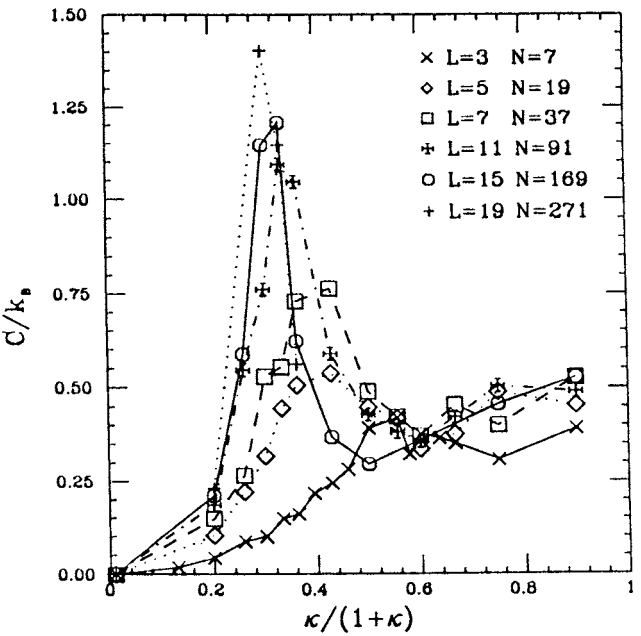

Fig. 7. Specific heat per monomer C as a function of bending rigidity κ for several values of L. The peak in the specific heat becomes more pronounced for larger L.

These MC results have been obtained for systems of quite limited size, and no attempt has been made to determine the critical exponents of the specific heat. The data is, however, sufficient to practically exclude the possibility of the first order phase transition (or, at least, to limit the possible latent heat to a very small value). Recently David and Guitter (1988) studied the behavior of rigid two-dimensional surfaces in large embedding dimension d, and recovered (to the first order in $1/d$) the second order phase crumpling transition. There is a reasonable quantitative agreement between those predictions and our MC results regarding the position of the critical point and the scaling behavior in the "semicrumpled" phase. On the other hand, a critical fluctuation analysis by an $\epsilon = 4 - D$ expansion, within Landau–Ginzburg theory (Paczuski *et al.*, 1988) predicts a first-order transition for $d < d_c = 219$. Such predictions, however, are not always reliable in the lowest order in ϵ.

4.2. *Excluded Volume Effects*

Excluded volume interactions may modify the details of the crumpling transition. In the flat phase, self-avoidance should be unimportant at long wavelengths. The main effect should be to augment the bending forces, thus delaying the transition to the crumpled state. In the crumpled phase, on the other hand, self-avoidance plays a major role of swelling the surface. The available numerical data (Kantor and Nelson, 1986, 1987) indicates that the excluded volume effects *are relevant* at the transition point, and thus we may expect a modification of the critical exponent, or even a change in the order of the transition. If the transition remains of second order, an interesting situation may appear: Just below the transition point ($\kappa \leq \kappa_c$), the density-density correlation function is expected to have a power-law dependence on the distance on length scales shorter than the correlation length ("semicrumpled" regime), just as in "regular" phase transitions. However, beyond the correlation length, we will *again* have a power-law regime determined by the behavior of self-avoiding flexible surfaces. Thus, instead of a crossover from a power-law to homogeneous regime, we will have a crossover between two different power-law regimes.

5. Concluding Remarks

5.1. *Summary and Discussion*

Our knowledge of the properties of tethered surfaces can be summarized in a few sentences: Flexible surfaces resemble linear polymers, and they can be treated by the methods which generalize the usual approach to polymers. This applies not only to the static, but also to the dynamic properties of flexible surfaces (Kantor *et al.*, 1986, 1987). As the rigidity of the surface increases, it undergoes a remarkable transition from a crumpled to flat state. Such a crumpling transition has no equivalent in the case of linear polymers.

The list of gaps in our knowledge is significantly longer: The problems begin at the earliest stage of transition from a microscopic Hamiltonian to its continuum version. Even in the case of a flexible phantom surface, we had to rely on MC results to justify the continuum form (2.12), and the subsequent use of the generalized Edwards' Hamiltonian (3.2). Similar problems prevent the proof of the validity of the recently suggested Hamiltonian (Paczuski *et al.*, 1988), which has been used to analyze the nature of crumpling transition within the framework of the Landau–Ginzburg theory. Although we understand the important qualitative features of the physics of tethered surfaces, our quantitative knowledge is quite limited: e.g., the value of the exponent ν has been established by MC investigations of very small systems, while the ϵ-expansion to the lowest order in ϵ did not produce a useful estimate of ν for a two-dimensional surface. We do not know the critical exponents, characterizing the crumpling transition, and can only speculate regarding the changes in the transition which will be caused by the excluded volume effects.

5.2. *What Next?*

Investigation of the behavior of the tethered surfaces presents an interesting and very rich problem. Presently, we only begin to understand the behavior of a *single* surface. Many questions of practical importance have yet to be answered. For example, it would be useful to know the physical properties of melts of surfaces, because, unlike linear polymers, tethered surfaces will not become ideal in a dense melt, since in their ideal (Gaussian) state they overfill the embedding space. Also, it would be interesting to find out the behavior of the surfaces near an adsorbing wall.

Two-dimensional membranes often exist as closed vesicles containing a volume of space, and this is a possibly important application of polymerized surfaces. Properties of such vesicles depend not only on the intrinsic properties of the membrane, but also on the pressure difference between their interior and the exterior. Behavior of a *linear* "vesicle" in $d = 2$ (i.e., a closed loop) has been recently investigated by Leibler *et al.* (1987). It would be very useful to extend those results to the more realistic case of two-dimensional tethered surface in $d = 3$.

Recently, it has been shown (Seung and Nelson, 1987) that a two-dimensional "solid" (i.e., a surface with a *finite* bond strength between the neighboring atoms or monomers) embedded in three dimensions, will melt, since the dislocation energy is finite in a surface, which is allowed to buckle in three dimensions. It is not known whether it will melt to a liquid or hexatic phase. Since the behavior of a surface depends on its in-plane order (in particular, hexatic membranes may undergo a crumpling transition (Nelson and Peliti, 1987)), it would be useful to have some way to compare the free energies of these two in-plane phases. Tethered surfaces provide a convenient "reference point" and may, probably, be used to compare these two phases. Melting of a two-dimensional "solid" in $d = 3$, has been analyzed under the assumption that in the absence of dislocations it is in the flat phase

(Nelson and Peliti, 1987; Seung and Nelson, 1988). It is not clear, what are the effects of the dislocations in the crumpled phase.

References

1. Alexander, S. and Orbach, R., *J. Physique Lett.* **43**, L625 (1982).
2. Aronovitz, J. A. and Lubensky, T. C., *Europhys. Lett.* **4**, 395 (1987).
3. Baumgärtner, A., in *Application of Monte Carlo Method in Statistical Physics*, ed. K. Binder (Springer, Berlin, 1984), p. 145.
4. Billoire, A., Gross, D. J. and Marinari, E., *Phys. Lett.* **139B**, 75 (1984).
5. Blumstein, A., Blumstein, R. and Vanderspurt, T. H., *J. Colloid Interface Sci.* **31**, 236 (1969).
6. Cates, M. E., *Phys. Rev. Lett.* **53**, 926 (1984).
7. Cates, M. E., *Phys. Lett.* **161B**, 363 (1985a).
8. Cates, M. E., *J. Physique* **46**, 1059 (1985b).
9. David, F. and Guitter, E., 1988 *preprint.*
10. Drouffe, J.-M., Parisi, G. and Sourlas, N., *Nucl. Phys.* **B161**, 397 (1979).
11. Duplantier, B., *Phys. Rev. Lett.* **58**, 2733 (1987).
12. Edwards, S. F., *Proc. Phys. Soc. London* **85**, 613 (1965).
13. Fendler, J. H. and Tundo, P., *Acc. Chem. Res.* **17**, 3 (1984).
14. Flory, D. J., *Statistical Mechanics of Chain Molecules* (Wiley, New York, 1979).
15. Frölich, J., in *Applications of Field Theory to Statistical Mechanics*, Vol. 216, ed. L. Garido (Springer, Berlin, 1985).
16. de Gennes, P. G., *Scaling Concepts in Polymer Physics* (Cornell University Press, Ithaca, New York, 1979).
17. Gomes, M. A. F., *J. Phys.* **A20**, L283 (1987).
18. Gross, D. J., *Phys. Lett.* **139B**, 187 (1984).
19. Helfrich, W., *J. Physique* **46**, 1263 (1985).
20. Helfrich, W., *J. Physique* **48**, 285 (1987).
21. Kadanoff, L. F., *Ann. Phys. (New York)* **100**, 359 (1976).
22. Kantor, Y., Kardar, M. and Nelson, D. R., *Phys. Rev. Lett.* **57**, 791 (1986).
23. Kantor, Y., Kardar, M. and Nelson, D. R., *Phys. Rev.* **A35**, 3056 (1987).
24. Kantor, Y. and Nelson, D. R., *Phys. Rev. Lett.* **58**, 2774 (1987a).
25. Kantor, Y. and Nelson, D. R., *Phys. Rev.* **A36**, 4020 (1987b).
26. Kardar, M. and Nelson, D. R., *Phys. Rev. Lett.* **58**, 1298 (1987).
27. Kardar, M. and Nelson, D. R., *Phys. Rev.* **A**, in press (1988).
28. Landau, L. D. and Lifshitz, E. M., *Theory of Elasticity* (Pergamon Press, New York, 1970).
29. Leibler, S., Singh, R. R. P. and Fisher, M. E., *Phys. Rev. Lett.* **59**, 1989 (1987).
30. Nelson, D. R. and Peliti L., *J. Physique* **48**, 1085 (1987).
31. Mandelbrot, B. B., *Fractals: Form Chance and Dimension* (Freeman, San Francisco, 1977).
32. Mandelbrot, B. B., *The Fractal Geometry of Nature* (Freeman, San Francisco, 1982).
33. Oono, Y., in *Adv. Chem. Phys.*, eds. I. Prigogine and S. A. Rice, Vol. LXI (Wiley, New York, 1981), p. 301.
34. Paczuski, M., Kardar, M. and Nelson, D. R., 1988, preprint.
35. Parisi, G., *Phys. Lett.* **81B**, 357 (1979).
36. Rammal, R. and Toulouse, G., *J. Physique Lett.* **44**, L13 (1983).
37. Seung, H. S. and Nelson, D. R., 1987, preprint.
38. Stephen, M. J., *Phys. Rev.* **B17**, 4444 (1978).
39. Weiner, J. H., *Statistical Mechanics of Elasticity* (Wiley, New York, 1983).